Materials Research. 2018; 22(2): e20180280
DOI: http://dx.doi.org/10.1590/1980-5373-MR-2018-0280

On the Global and Localised Corrosion Behaviour of the AA2524-T3 Aluminium Alloy Used as Aircraft Fuselage Skin

***Jéferson Aparecido Moreto*[a], *Luciana Sgarbi Rossino*[b], *Waldek Wladimir Bose Filho*[c], *Cláudia Eliana Bruno Marino*[d], *Miguel da Conceição Ferreira*[e], *Maryna Taryba*[e], *João Carlos Salvador Fernandes*[e,f]**

[a]*Instituto de Ciências Exatas, Naturais e Educação, Universidade Federal do Triângulo Mineiro (UFTM), Av. Doutor Randolfo Borges Júnior, 38064200, Uberaba, MG, Brasil*
[b]*Universidade Federal de São Carlos - UFSCar, Rodovia João Leme dos Santos, Km 110, Bairro do Itinga, 18.052-780, Sorocaba, SP, Brasil*
[c]*Departamento de Engenharia de Materiais, Universidade de São Paulo, Av. Trabalhador São-carlense, 400, 13566590, São Carlos, SP, Brasil*
[d]*Departamento de Engenharia Mecânica, Universidade Federal do Paraná (UFPR), Av. Cel. Francisco H. dos Santos, 230, 81531990, Jardim das Américas, Curitiba, PR, Brasil*
[e]*Centro de Química Estrutural - CQE, Instituto Superior Técnico, Universidade de Lisboa, 1049-001, Lisboa, Portugal*
[f]*Departamento de Engenharia Química, Instituto Superior Técnico, Universidade de Lisboa, 1049-001, Lisboa, Portugal*

Received: April 15, 2018; Revised: October 22, 2018; Accepted: November 20, 2018

The aim of this work was to study the corrosion process of new aluminium alloy AA2524-T3 (Solution Heat Treated and Cold Worked), which is a promising substitute of the base line AA2024-T3 for aircrafts fabrication, by global and localised techniques in sodium chloride medium (0.05 mol L^{-1} NaCl). The open circuit potential results revealed a stochastic evolution of pitting events and to the resulting variations in the ratio of passive/active areas and/or cathode/anode, which may be related to the presence of different types of intermetallics. The cyclicvoltammetry showed that the corrosion potential (E_{corr}) and the pit nucleation potential (E_{pit}) values are quite similar (approximately -0.525 V). The results of EIS show that the corrosion rate is quite stable, with no tendency to increase or decrease for longer immersion periods. The results of SVET were in agreement with the results obtained by EIS technique, showing strong anodic activity on the surface with no repassivation along the whole immersion time. Besides, corrosion process led to significant surface degradation after 24h.

Keywords: *Galvanic coupling, Intermetallics, Pitting, EIS, SVET.*

1. Introduction

Applications of Al alloys increase day by day, with great emphasis in the areas of transportation, civil construction, packaging and energy transportation [1,2]. Al alloys have become attractive due to their low cost, low density, mechanical and corrosive properties [3,4]. As described by Eskin [5] in commercial 2xxx series aluminium alloys, Cu and Mg are the main alloying elements with small amount of Si and other minor elements as Zn, Mn, Ti and Fe. The Cu alloying element provides one of the most widely used mechanisms for the strengthening [6]. According to the American Society for Metals [2] the alloys of the 2xxx series are particularly suitable for structural parts that require a high strength-to-weight ratio and are used in the manufacture of aircraft fuselages, aircraft wings and parts needing a good resistance to temperatures below 150 ºC. However, as described by Queiroz et al. [7] and Bonfils-Lahovary et al. [8], aluminium alloys have a very complex microstructure due to heterogeneities leading to an increase of localised corrosion.

In order to improve the durability of the aircrafts, the aeronautical industry has been constantly working on development of new advantageous aluminium alloys [9]. The AA2524-T3 (Solution Heat Treated and Cold Worked) alloy produced by ALCOA may be used as fuselage skin material and represents a potential replacement for the AA2024 alloy, widely used by the aircraft industry [9]. Recent publications showed that the fatigue behaviour of AA2524-T3 aluminium alloy is dependent on experimental conditions (e.g. applied stress, loading rate, etc.) as well as sample orientation [10,11]. However, susceptibility to corrosion of AA2524-T3 alloy requires additional studies and the effect of the intermetallics (IMs) on the pitting corrosion of this alloy is still not fully understood.

Studies developed by Birbilis et al [12,13] confirm that the electrochemical characteristics of IMs vary significantly in terms of corrosion potential, disintegration, oxygen reduction and dissolution reactions. As mentioned by Boag et al [14] the

*e-mail jeferson.moreto.uftm@gmail.com

IMs particles can be anodically or cathodically polarized with respect to the Al matrix, being preferentially corroded or inducing corrosion of the nearby matrix, respectively. In a previous work [12], we studied the corrosion resistance of two novel alloys developed for aircraft industry (AA2198-T851 and 7081-T73511) to that presented by the alternative base alloys (AA2524-T3 and 7050-T7451, respectively). Regarding to 2xxx series Al alloys, the results confirmed that AA2198-T851 might show a superior corrosion performance compared to AA2524-T3 and the localised corrosion is related to the existence of IMs particles.

In this paper, the global and localised corrosion resistance of the AA2524-T3 aluminium alloy has been investigated by immersion test in 0.05 mol L^{-1} NaCl solution. It is important to note that the present manuscript is complementary to the results obtained previously [15]and reveals more details on the corrosion behaviour of the AA2524-T3 alloy used as fuselage skin material. For this purpose, the open circuit potential (OCP), potentiodynamic polarization (PP), cyclic potentiodynamic polarization, electrochemical impedance spectroscopy (EIS) and scanning vibrating electrode techniques (SVET) were performed.

2. Material e Methods

For the present investigations, the AA2524-T3 aluminium alloy (produced by ALCOA) was used in the "as received" condition. Table 1 lists the chemical composition of its major elements. Specimens of AA2524-T3 aluminium alloy were wet ground using abrasive papers from 800# to 4000#. Prior to testing, they were degreased with propanol and carefully rinsed with distilled water. The morphology and composition of the alloy surface were assessed by scanning electron microscopy (SEM) before and after the corrosion tests, using an analytical FEG-SEM JEOL 7001F equipped with an Oxford light elements EDS detector.

The open circuit potential (E_{ocp}) of the samples was monitored during 3600 s. Cyclic potentiodynamic polarization curves were recorded according to the ASTM G61-86 standard [16] in the positive direction at a scan rate of 0.6 V h^{-1}. As described by the ASTM G61-86 [16] standard the onset of localised corrosion is usually marked by a rapid increase of the anodic current at potentials below the oxygen-evolution potential. When the current reaches 5 mA cm^{-2}, the scanning direction is reversed. The test was concluded when negative values of the current were again recorded.

Table 1. Composition of the aluminium alloys (wt %).

Elements	AA2524-T3
Cu	3.84 (4.0 – 4.5)
Si	0.04 (0.06 max)
Fe	0.06 (0.12 max)
Mg	1.312 (1.2 – 1.6)
Mn	0.56 (0.45 – 0.9)
Ti	0.029 (0.1 max)
Zn	0.01 (0.15max)
Cr	ND (0.05max)
Al	Balance

OBS: measured and (nominal) values.

ND: unidentified

EIS spectra were obtained for AA2524-T3 aluminium alloy in the frequency range from 66 kHz to 10 mHz, using a sinusoidal perturbation of 10 mV (rms). In the present study, the spectra were obtained at 20 mV negative to E_{corr}, in order to avoid non-linearity problems related with the occurrence of pitting at the corrosion potential [17]. The EIS measurements were performed in triplicate after 1, 3, 8, 12, 24, 48, 120 and 168 h of immersion. The consistency of the impedance data and compliance to the validation criteria for these measurements was assessed through the use of KK transforms. For EIS data fitting, the ZView2© software was used. All the above electrochemical experiments were conducted in a naturally aerated solution of 0.05 mol L^{-1} NaCl at 25±1 ºC, using a classical three-electrode configuration: the AA2524-T3 aluminium alloy as working electrode with an exposed area of 0.38 cm^2, a saturated calomel reference electrode (Hg/Hg_2Cl_2, KCl_{sat}) and a platinum auxiliary electrode.

The SVET tests were performed up to 24 h of immersion in a 0.05 mol L^{-1} NaCl naturally aerated solution at room temperature, using a SVET system from Applicable Electronics Inc., controlled by the ASET software (Sciencewares, Inc.). To perform the measurements, the sample was glued to a holder and the exposed area (a square of approximately 0.6-1 mm^2) was delimited by insulating the remaining surface using a mixture of beeswax and colophony. The visual appearance of the exposed area was continuously assessed with a microscopic video system with 140 times magnification. Measurements were performed in a 26 x 26 grid generating 676 data points. An insulated Pt-Ir probe with platinum black deposited on a spherical tip was used as vibrating electrode. The diameter of the sensing probe tip was 18µm. The probe was placed 100 µm above the surface, vibrating in 2 perpendicular planes, vertical (Z) and horizontal (X). The vibration frequencies of the probe were 124 Hz (Z) and 325 Hz (X). The measuring step has varied from 26 to 40 µm, depending of the size of the surface exposed to solution.

3. Results e Discussion

The dimension, type, and distribution of IMs particles are very important factors that affect the mechanical and corrosion-resistance performance of AA2524-T3 aluminium alloy. The microstructure of the AA2524-T3 alloy consists of a solid solution of Al and dispersion of incoherent particles in the matrix. Two types of IMs were found: T1 (Al, Cu, Mn and Fe) and incoherent precipitates T2 (Al, Cu, Mg) as

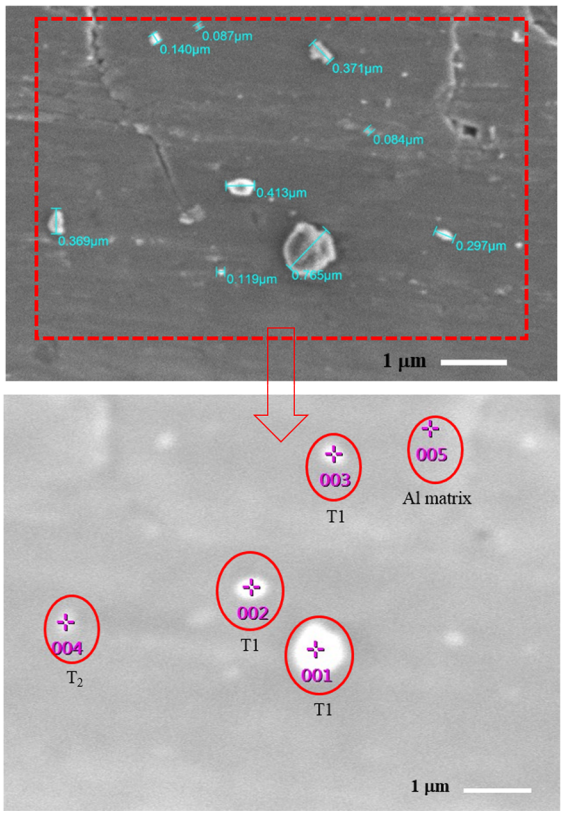

Figure 1. SEM observation of the 2524-T3 aluminium alloy before the electrochemical tests.

can be seen in Figure 1. The knowledge of the intermetallic compounds present in the AA2524-T3 alloy is extremely important since the corrosion resistance of aluminium alloys depends on their composition metal heterogeneities and on the medium or exposure conditions. These IMs usually cause localized corrosion such as pitting corrosion, due to the electrochemical potential difference between the IMs and the matrix. A detailed study of the IM compounds present in the AA2524-T3 alloy are in line with the previous work presented elsewhere [9,15,18-19].

As reported by Srivatsan [20], the microstructure of the AA2524-T3 aluminium alloy is fully recrystallized, presenting elongated and flattened grains. The EDS spectra used for the determination of the IMs compositions are not shown. Zheng *et al.*[21] studied the behaviour of fatigue crack initiation and propagation in AA2524-T3 alloy. According to those authors, the SEM observation demonstrated that a large number of second phase particles parallel to the rolling direction can be found in the alloy. With the help of Energy-dispersive X-ray spectroscopy (EDS) analysis the same authors have obtained the chemical composition of these particles, consisting of some large particles containing Al, Cu, Fe, Mn and smaller particles containing Al, Cu and Mg. These precipitates usually cause localised corrosion such as pitting corrosion and intergranular corrosion, due to the electrochemical potential difference between the precipitates and the matrix.

A representative curve of the open circuit potential (OCP) evolution with the immersion time for the AA2524-T3 aluminium alloy is presented in Figure 2 (a).The dependence of potential with time is linked to the stochastic evolution of pitting events and to the resulting variations in the ratio of passive/active areas and/or cathode/anode, which may be related to the presence of different types of intermetallics [15]. Gamboni *et al.*[22] studied the corrosion behaviour of AA2524-T3 aluminium alloy in 3.5 % NaCl solution (0.6 mol L^{-1}), showing that the corrosion potential of this alloy is -0.634 V. In the present work, the open circuit potential of AA2524-T3 aluminium alloy is approximately -0.525 V after 3600 s of immersion and just before the cyclic voltammetry test. This observation is consistent with other investigations performed in Al alloys, taking into account the lower chloride concentration used. Figure 2 (b)shows a low magnification optical microscopy image of the surface after the open circuit potential test, where a large number of pits can be observed, providing valuable information on the on the nature of the corrosion process.

Figure 3 (a)presents the characteristic cyclic voltammetric curve for the 2524-T3 aluminium alloy in 0.05 mol L^{-1} NaCl aqueous solution and Figure 3 (b) the magnified area for determining the pit nucleation potential (E_{pit}). Figure 3 (c) shows the optical micrograph after the test. The corrosion potential (E_{corr}) and E_{pit} values are approximately equal. It is important to mention the E_{pit} was obtained from the extrapolation of the linear portion of the ascending curve. Almost no passive plateau can be observed in the anodic domain, suggesting growth of pits with the surge of current. According to Szklarska-Smialowska [23] when the films formed on the surfaces of aluminium alloys are exposed to Cl^- ions, fractures occur at specific points, leading to pits. Buchheit *et al.*[24] studied the pit nucleation potential exhibited by simulated intermetallics with various compositions. The obtained values were compared with the experimental values observed for the AA2024-T3 aluminium alloy. The author verified that a part of the IMs exhibited a potential lower than the alloy, concluding that the beginning of pitting corrosion of the alloy is probably associated with the selective dissolution of the IMs.

Since the passive film is broken, the process of dissolution/ corrosion is initiated, causing the increase of the current density. When the current reaches 5 mA cm^{-2}, the scanning direction was reversed and in this region it is possible to observe the presence of hysteresis as the current density in the cathodic direction is higher than in the anodic direction. Although an inflexion of the curve is noticed at approximately -0.53 V, characteristic of possible repassivation of the active pits, no passive plateau is observed in this reverse region, indicating that a complete repassivation was not achieved. For a more concentrated electrolyte (0.6 M) the pitting

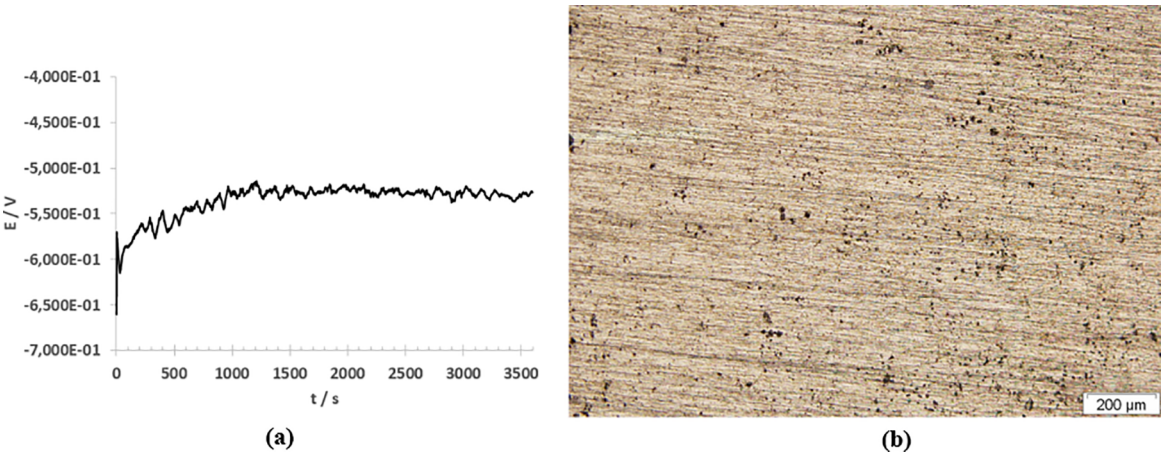

Figure 2. (a) Open circuit potential curve of the AA2524-T3 aluminium alloy in aerated 0.05 mol L^{-1} NaCl aqueous solution and **(b)** image of AA2524-T3 aluminium alloy by optical microscopy of surface after the open circuit potential test.

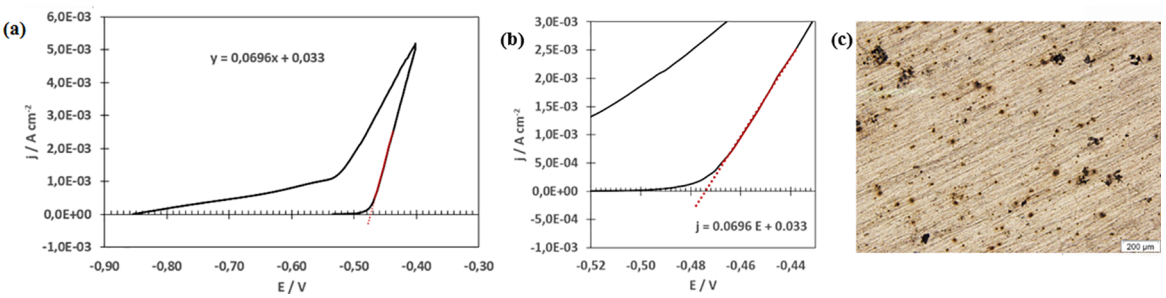

Figure 3. (a) Cyclic potentiodynamic polarization curve of the AA2524-T3 aluminium alloy in aerated 0.05 mol L^{-1} NaCl aqueous solution, (b) the magnified area for determining the pit nucleation potential (E_{pit}=-0.474 V) and (c) image of AA2524-T3 aluminium alloy by optical microscopy of surface after the cyclic potentiodynamic polarization test.

potential was around -0.63 V [22]. In Figure 3 (c),obtained by optical microscopy, it is possible to notice pitting corrosion.

SEM observation of the AA2524-T3 aluminium alloy after the OCP tests (Figure 4 (a)) revealed the presence of IMs whose elemental chemical composition was obtained through EDS analysis. Probably, the intermetallic shown in the micrograph is T_1 (Al, Cu, Fe, Mn). Figure 4 (b)presents the SEM observation after the PP tests. As can be seen, the presence of cathodic T_2 (Al, Cu, Mg) promotes galvanic coupling, leading to the preferential dissolution (trenching) of the nearby matrix and formation of preferential sites for pitting initiation. The micrograph also presents defects and pitting in the surface of material.

EIS spectra were obtained for, at least, three samples of AA2524-T3 aluminium alloy after 1, 3, 8, 12, 24, 48, 120 and 168 h of exposure to the 0.05 mol L^{-1} NaCl solution. Figure 5 (a)shows a comparison of the data obtained for alloy AA2524-T3 in this work and the data obtained by Moreto et al [12] in 0.6 mol L^{-1} NaCl aqueous solution after 24 h exposure. As can be seen, in both conditions the electrochemical behaviour of the AA2524-T3 alloy suggested two time constants, one at high frequencies and a second time constant at lower frequencies. According to Ferreira et al [25] the second time constant is due to localised corrosion processes. As reported by Yasakau et al [26] localised corrosion is a very complex process involving many heterogeneous and homogeneous reactions. Ma et al. [27] studied the localised corrosion of AA2099-T83 Al - Li alloys, concluding that the localised corrosion associated with low-copper containing Al-Fe-Mn-Cu- (Li) particles is typified with trenching around the particles. In the present case, the characteristic time constant at low frequencies is clearly due to pitting corrosion, which is also evident in Figure 5 (b), where the evolution of potential with time during the first hour shows the typical transients of this type of corrosion. The main difference between the results in the two different solutions is the higher impedance moduli at high frequencies observed in 0.05 mol L^{-1} NaCl solution, due to the lower conductivity of this solution. The impedance moduli at low frequencies are very similar, indicating a low resistance to localised corrosion in both cases.

The equivalent circuit depicted in Figure 6 (a), based on the circuit originally presented by Jüttner [28] may be used to describe the behaviour of this kind of materials. It is composed by R_Ω, ohmic resistance of the electrolyte, a loop R_{ox}-C_{ox}, respectively the resistance and capacitance of

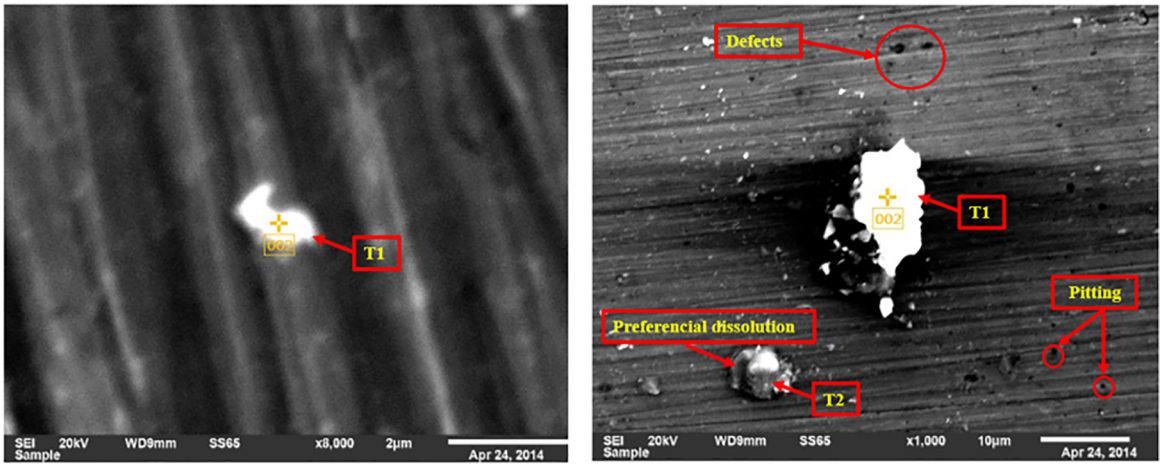

Figure 4. (a) SEM observation of the AA2524-T3 aluminium alloy after the open circuit potential tests and (b) SEM observation of the AA2524-T3 aluminium alloy after the potentiodynamic polarization tests.

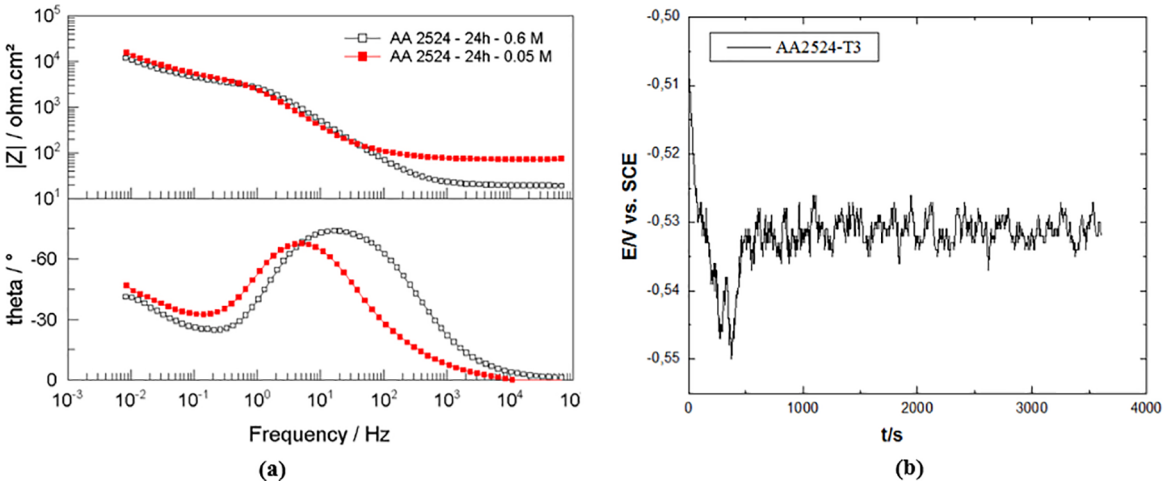

Figure 5. (a) Comparison of the data obtained for alloy AA2524-T3 in this work (mol L^{-1}) and the data obtained by Moreto *et al*[12] in 0.6 mol L^{-1} NaCl solution after 24 h exposure and (b) evolution potential with time for the first hours of tests.

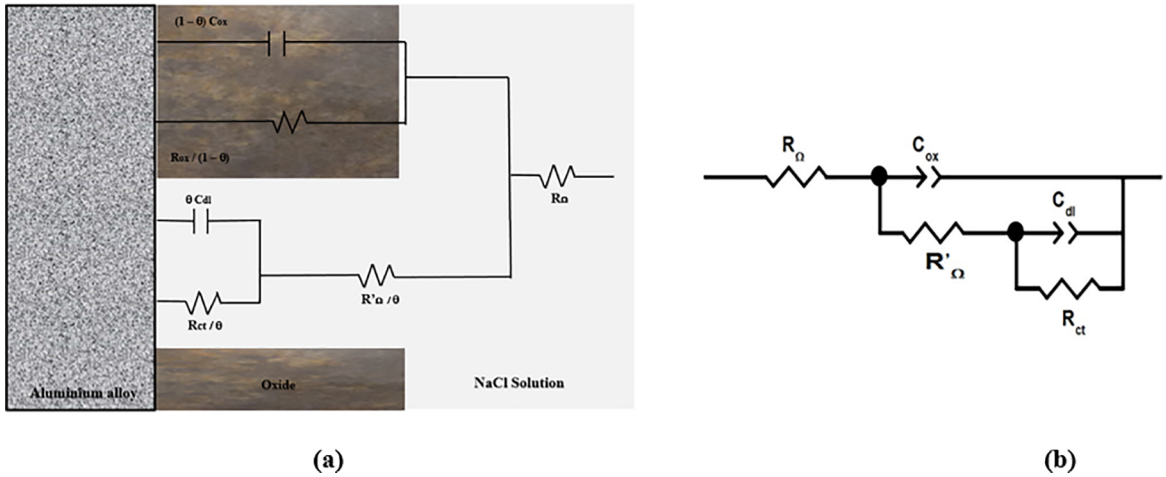

Figure 6. (a) Schematic representations of the model 25 and (b) proposed equivalent circuit.

the oxide layer, and a contribution of the pitting/trenching processes taking place at the particles as a R_{ct}-C_{dl} network that represents the charge transfer reaction corresponding to localised corrosion and the capacitance of the double layer, added to the additional resistance of the electrolyte inside the pit/trench, R'_{Ω}. The measured values R_{ox}, C_{ox}, R'_{Ω}, R_{ct} and C_{dl} depend on the pitted area fraction θ and so they correspond to $R^*_{ox}/(1-\theta)$, $(1-\theta)C^*_{ox}$, $R^{*\prime}_{\Omega}/\theta$, R^*_{ct}/θ and θC^*_{dl}, where R^*_{ox}, C^*_{ox}, $R^{*\prime}_{\Omega}$, R^*_{ct} and C^*_{dl} are the intrinsic values of each parameter. As $R_{ox}/(1-\theta)$ tends to be extremely high, not allowing for any conduction of electrons across the oxide film, this circuit element is usually removed from the equivalent circuit, that transforms into the one proposed by Mansfeld and Kendig [29], depicted in Figure 6 (b).

Table 2shows the average values of the EIS parameters of AA2524-T3 aluminium alloy in 0.05 mol L^{-1} NaCl solution. The values of R_{Ω} show a constant decrease with time, explained by the evaporation of water in the cell during the 168 h of tests, leading to an increase of concentration and, thus, conductivity with time. The analysis of C_{dl} values shows a tendency towards higher values as the immersion time increases. This could be attributed to the increase of the pitted area,θ, as C_{dl} is, in fact, the product of an intrinsic capacitance C^*_{dl} by the pitted to total surface ratio. However, such an increase of the pitted area would in principle lead to a decrease in the resistance R_{ct}, which is not observed. An alternative explanation may be related with the extreme pH values expected inside the pits. In fact, it is commonly accepted that the intrinsic interfacial capacitance tends to increase as the local environment inside the pits turns more aggressive.

According to Ahmed [30], as the pH decreases below the pH_{pzc} of aluminium oxide, the adsorption of anions will lead to an exponential increase of the capacitance. This effect was also studied by Fernandes [31] in W-implanted aluminium. Finally, the evolution of the pits or trenches may be affected by the formation of corrosion products that block the surface, justifying the decrease in the capacitance values for very long immersion times. Concerning the values of R_{tc}, they show an initial increase, followed by stabilization in the range of 60-70 kΩ cm^2.

The results of SVET measurements are presented in Figure 7, where (a) and (b) correspond to optical micrographs at the beginning and after 24 h of immersion, respectively, and (c), (d) and (e) depict the current density distributions after 1h, 14h and 20 h. As it can be seen in Figure 7 (c), the sites of anodic activity were detected from the very beginning of immersion and were continuously developing along the immersion time (Figure 7 (d) and (e)). The maximum values of cathodic current density remained stable from one scan to the other during the whole period of measurements (Figure 7 (c)-(e)).No passivation was observed. After 24h of immersion significant degradation of surface was evident (Figure 7 (b)). The results demonstrate that the zone of the preferential formation of pits correlates to the zone recognized by SVET as a cathodic. Shi et al in [32] conclude that self-dissolution of S phase plays prevalent role in corrosion process resulting in trenching of aluminium matrix around S-phase intermetallics and formation of the pits.

4. Conclusions

An experimental investigation of the corrosion behaviour of industrially important AA2524-T3 aluminium alloy, used in aircraft fabrication, was performed in diluted 0.05 mol L^{-1} NaCl solution. Two conclusions were obtained in this work:

1. The pitting resistance of the alloy is considered low and quite similar to those obtained in 0.6 mol L^{-1} (or 3.5%) NaCl solution, so even a reduced chloride concentration promoted pitting;
2. The evolution of the process with time was assessed, showing that the corrosion rate is quite stable, with no tendency to increase or decrease for longer immersion periods. The results of SVET were in agreement with the results obtained by general electrochemical techniques, demonstrating no passivation along the whole immersion time. Besides, corrosion process led to significant surface degradation after 24 h.

5. Acknowledgements

The authors gratefully acknowledge the Department of Mechanical Engineering - Federal University of Paraná

Table 2. Average values of the EIS parameters of AA2524-T3 aluminium alloy obtained by Zview 2 software.

Sample	Time (h)	R_{Ω} ($\Omega.cm^2$)	C_{ox} ($\mu F.cm^{-2}$)	R'_{Ω} ($k\Omega.cm^2$)	C_{dl} ($\mu F.cm^{-2}$)	R_{ct} ($k\Omega.cm^2$)
	1	92.54	40.3	8.52	113	31.85
	3	92.95	58.3	6.13	258	49.90
	8	91.08	66.6	5.57	645	64.46
AA2524	12	80.57	71.1	4.49	856	67.41
	24	75.30	72.8	5.29	632	64.28
	48	73.93	91.6	5.92	393	48.65
	120	75.26	148	6.38	348	64.85
	168	64.59	179	6.13	339	69.08

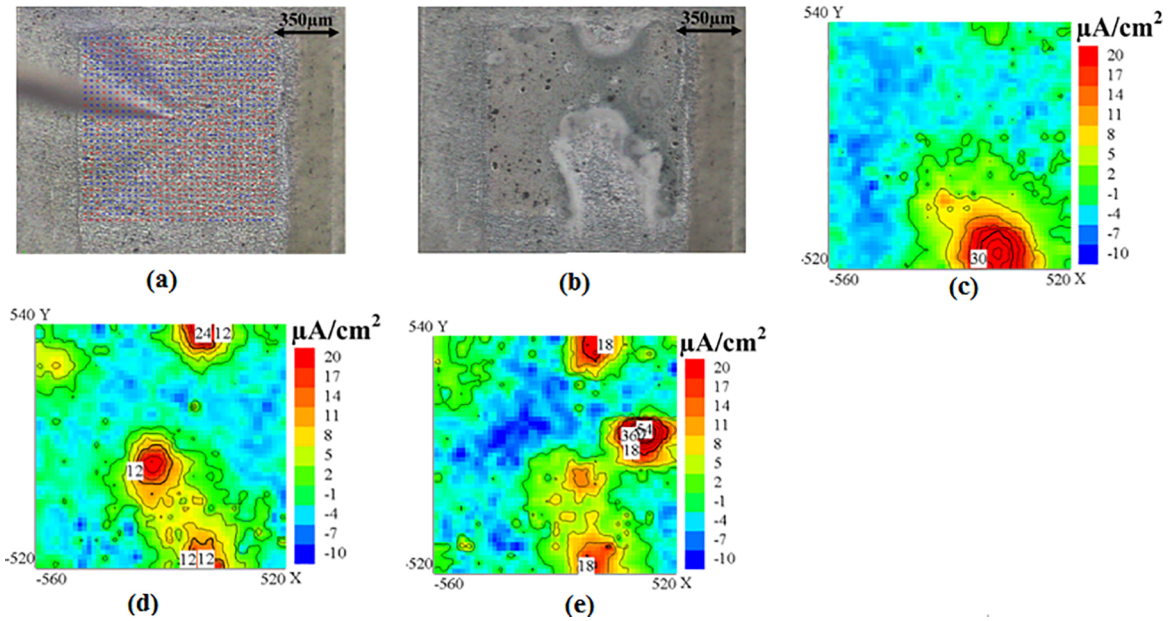

Figure 7. SVET results along 24 h immersion in 0.05 mol L^{-1} NaCl solution. **(a)** optical micrograph at the beginning of immersion depicting grid points; **(b)** optical micrograph after 24h of immersion; **(c)**, **(d)** and **(e)** current density distributions after 1 h, 14 h and 20 h of immersion respectively. X and Y coordinates represent the length of the mapping in µm.

(UFPR), Department of Materials Engineering, University of São Paulo - USP and CQE / Instituto Superior Técnico-University of Lisbon for providing the laboratories facilities, as well as the financial support by Fundação para a Ciência e Tecnologia (FCT) to CQE under contract UID/QUI/00100/2013, National Counsel of Technological and Scientific Development (Processes: 303684/2015-1 and 402142/2016-0).

6. References

1. Steglich D, Wafai H, Besson J. Interaction between anisotropic plastic deformation and damage evolution in Al 2198 sheet metal. *Engineering Fracture Mechanics*. 2010;77(17):3501-3518.

2. ASM International. *ASM Metals Handbook Volume 2: Properties and Selection: Nonferrous Alloys and Special-Purpose Materials*. Materials Park: ASM International; 1990. p. 17-22.

3. Totten GE, Mackenzie DS, eds. *Handbook of Aluminum: Volume 1: Physical Metallurgy and Process*. Boca Raton: CRC Press; 2003.

4. Shen F, Yi D, Jiang Y, Wang B, Liu H, Tang C, et al. Semi-quantitative evaluation of texture components and fatigue properties in 25244-T3 aluminum alloy sheets. *Materials Science & Engineering: A*. 2016;657:15-25.

5. Eskin DG. Decomposition of supersaturated solid solutions in Al-Cu-Mg-Si alloys. *Journal of Materials Science*. 2003;38(2):279-290.

6. Ghosh KS, Hilal M, Bose S. Corrosion behavior of 2024 Al-Cu-Mg alloy of various tempers. *Transactions of Nonferrous Metals Society of China*. 2013;23(11):3215-3227.

7. Queiroz FM, Magnani M, Costa I, de Melo HG. Investigation of the corrosion behaviour of AA2024-T3 in low concentrated chloride media. *Corrosion Science*. 2008;50(9):2646-2657.

8. Bonfils-Lahovary ML, Lanffont L, Blanc C. Characterization of intergranular corrosion defects in a 2024-T351 aluminium alloy. *Corrosion Science*. 2017;119:60-67.

9. Gamboni OC, Moreto JA, Bonazzi LHC, Ruchert COFT, Bose Filho WW. Effect of salt-water fog on fatigue crack nucleation of Al and Al-Li alloys. *Materials Research*. 2014;17(1):250-254.

10. Chen YQ, Pan SP, Zhou MZ, Yi DQ, Xu DZ, Xu YF. Effects of inclusions, grain boundaries and grain orientations on the fatigue crack initiation and propagation behaviour of 2524-T3 Al alloy. *Materials Science & Engineering: A*. 2013;580:150-158.

11. Golden PJ, Grandt AF Jr., Bray GH. A comparison of fatigue crack formation at holes in 2024-T3 and 2524-T3 aluminum alloy specimens. *International Journal of Fatigue*. 1999;21(Suppl 1):S211-S219.

12. Birbilis N, Buchheit RG. Electrochemical Characteristics of Intermetallic Phases in Aluminum Alloys: An Experimental Survey and Discussion. *Journal of the Electrochemical Society*. 2005;152(4):B140-B151.

13. Birbilis N, Cavanaugh MK, Buchheit RG. Electrochemical behaviour and localized corrosion associated with Al_7Cu_2Fe particles in aluminum alloy 7075-T651. *Corrosion Science*. 2006;48(12):4202-4215.

14. Boag A, Hughes AE, Glenn AM, Muster TH, McCulloch D. Corrosion of AA2024T3 Part I: Localised corrosion of isolated IM particles. *Corrosion Science*. 2011;53(1):17-26.

15. Moreto JA, Marino CEB, Bose Filho WW, Rocha LA, Fernandes JSC. SVET, SKP and EIS study of the corrosion behaviour of high strength Al and Al-Li alloys used in aircraft fabrication. *Corrosion Science*. 2014;84:30-41.

16. ASTM International. *ASTM G61-86(2014) - Standard Test Method for Conducting Cyclic Potentiodynamic Polarization Measurements for Localized Corrosion Susceptibility of Iron-, Nickel-, or Cobalt-Based Alloys*. West Conshohocken: ASTM International; 2014.

17. Mansfeld F, Fernandes JCS. Impedance spectra for aluminum 7075 during the early stages of immersion in sodium chloride. *Corrosion Science*. 1993;34(12):2105-2108.

18. Moreto JA, Gamboni OC, Marino CEB, Bose Filho WW, Fernandes JCS, Rocha LA. Corrosion behaviour of Al and Al-Li alloys used as aircraft materials. *Corrosão e Protecção de Materiais*. 2012;31(3/4):60-64.

19. Moreto JA, Broday EE, Rossino LS, Quites FJ, Fernandes JCS, Bose Filho WW. Effect of Localized Corrosion on Fatigue Crack Growth in 2524-T3 and 2198-T851 Aluminum Alloys Used as Aircraft Materials. *Journal of Materials Engineering and Performance*. 2018;27(4):1917-1926.

20. Srivatsana TS, Kolara D, Magnusen P. The cyclic fatigue and final fracture behaviour of aluminum alloy 2524. *Materials & Design*. 2002;23(2):129-139.

21. Zheng ZQ, Cai B, Zhai T, Li SC. The behaviour of fatigue crack initiation and propagation in AA2524-T3 alloy. *Materials Science and Engineering: A*. 2011;528(4-5):2017-2022.

22. Gamboni OC. *Estudo do efeito do ambiente no comportamento em fadiga de novas ligas de AL de grau aeronáutico*. [Dissertation]. São Carlos: University of São Paulo; 2011.

23. Szklarska-Smialowska Z. *Pitting corrosion of aluminum*. Corrosion Science. 1999;41(9):1743-1767.

24. Buchheit RG. The Electrochemistry of θ (Al_2Cu), S (Al_2CuMg) and T_1 (Al_2CuLi) and Localized Corrosion and Environment Assisted Cracking in High Strength Al Alloys. *Material Science Forum*. 2000;331-337:1641-1646.

25. Ferreira SC, Rocha LA, Ariza E, Sequeira PD, Watanabe Y, Fernandes JCS. Corrosion behaviour of Al/Al_3Ti and Al/Al_3Zr functionally graded materials produced by centrifugal solid-particle method: Influence of the intermetallics volume fraction. *Corrosion Science*. 2011;53(6):2058-2065.

26. Yasakau KA, Zheludkevich ML, Lamaka SV, Ferreira MGS. Mechanism of Corrosion Inhibition of AA2024 by Rare-Earth Compounds. *The Journal of Physical Chemistry B*. 2006;110(11):5515-5528.

27. Ma Y, Zhou X, Huang W, Thompson GE, Zhang X, Luo C, et al. Localized corrosion in AA2099-T83 aluminum-lithium alloy: The role of intermetallic particles. *Materials Chemistry and Physics*. 2015;161:201-210.

28. Jüttner K. Electrochemical impedance spectroscopy (EIS) of corrosion processes on inhomogeneous surfaces. *Electrochimica Acta*. 1990;35(10):1501-1508.

29. Kendig MW, Mansfeld F. AC electrochemical impedance of a model pit. *Journal of the Electrochemical Society*. 1982;129:C318.

30. Ahmed SM. Electrical Double Layer at Metal Oxide- Solution Interfaces. In: Diggle JW, Vijh AK, eds. *Oxides and Oxide Films - Volume I*. New York: Marcel Dekker; 1972. p. 475

31. Fernandes JCSS. *Corrosão por picadas em alumínio modificado por implantação iónica de tungsténio*. [PhD Thesis]. Lisbon: Instituto Superior Técnico; 1997.

32. Shi H, Tian Z, Hu T, Liu F, Han EH, Taryba M, et al. Simulating corrosion of Al_2CuMg phase by measuring ionic currents, chloride concentration and pH. *Corrosion Science*. 2014;88:178-186.